Photon angular distribution in two-photon electron capture by H-like uranium

Konstantin N. Lyashchenko [1,2,3] Oleg Yu. Andreev [1,2] and Deyang Yu [3,4]

[1]*Division of Quantum Mechanics, St. Petersburg State University, 7/9 Universitetskaya naberezhnaya, St. Petersburg 199034, Russia*

[2]*Petersburg Nuclear Physics Institute Named by B.P. Konstantinov of National Research Centre "Kurchatov Institute," mikro rayon Orlova roshcha 1, Gatchina, 188300 Leningrad District, Russia*

[3]*Institute of Modern Physics, Chinese Academy of Sciences, Lanzhou 730000, China*

[4]*University of Chinese Academy of Sciences, Beijing 100049, China*

(Received 28 November 2024; accepted 25 February 2025; published 20 March 2025)

We present a comprehensive study of the angular distribution of photons emitted during resonant two-photon electron capture by H-like uranium ions. Focusing on the energies of incident electrons, for which the dielectronic recombination (DR) dominates, we analyze the angular emission spectrum of the most significant cascade transitions, which make the main contribution to the total cross section. In particular, we consider the cascade transitions that occur with the formation of $(1s2s)$ and $(1s2p)$ intermediate states. We investigate the angular distribution of the emitted photons beyond the single-photon approximation. We separately consider the contributions of the DR and the radiative recombination channels and demonstrate that the two-photon angular distribution shows strong interference between these channels.

DOI: 10.1103/PhysRevA.111.032815

I. INTRODUCTION

Radiative electron transitions in atoms and ions are fundamental processes in atomic physics, governing much of the behavior of matter under various physical conditions. Among these processes, one- and two-photon transitions play an important role, particularly in the emission of radiation during electron capture. Although the energy spectrum of these emissions has been widely studied [1–4], the angular distribution of the emitted photons, especially for two-photon processes, has received comparatively less attention. Understanding the angular distribution is crucial because it provides deeper insight into the dynamics of photon emission and the underlying atomic interactions, providing more detailed information than spectral measurements alone [5].

The photon angular distribution of the one-photon radiative transitions during electron capture was extensively investigated [5,6]. However, the photon angular distribution of the two-photon electron capture, in particular involving dielectronic recombination (DR), has not been studied in detail. Most of the theoretical works on the DR were limited by the single-photon approximation [7–10], where only the emission of the resonant photon was considered. Within the framework of the single-photon approximation, it is impossible to investigate the continuous nature of the emission spectrum and take into account the complex angular correlations between the emitted photons. In Ref. [11], the resonance approximation (disregarding interference between photons) was employed to investigate the two-photon angular distribution of the two-photon DR with H-like uranium. In particular, the angular distribution of the second photon, emitted in the $(1s2p_{1/2})_1 \to (1s^2)$ transition, for the DR with the formation of the $(2p_{1/2}2p_{3/2})$ autoionizing states was calculated. A comprehensive study of the full two-photon angular distribution free from these constraints is therefore essential for understanding the photon interaction mechanisms.

Radiative electron capture, in which only the radiative recombination (RR) channel is dominant, has been thoroughly investigated in many atomic systems. However, in systems with two or more electrons, the DR channel becomes crucial, attracting considerable attention from experimenters [1–3,9,12–15]. The DR not only is relevant for understanding atomic systems but also plays a key role in describing laboratory plasmas and astrophysical phenomena [16]. The first measurements of the DR cross section were presented in [9,12], in which the experimental results validate theoretical predictions about the substantial influence of the Breit interaction and the interference between resonances. Recently, experimental research has shifted to investigating the energy spectra of emitted photons in DR [1–3]. Notably, the photon emission spectra for DR in H-like and He-like iron [1,2] and Be-like lead [3] ions were measured, focusing on the continuous nature of the two-photon emission spectrum. This was a significant step in experimental research, providing new insights into the complexities of two-photon processes and serving as motivation for this theoretical investigation.

Building on our previous work [4], in which we investigated the energy emission spectrum of resonant two-photon electron capture, this study focuses on the photon angular distribution of photons emitted during the same process in H-like ions. Two-photon processes exhibit rich angular correlations that reveal a complex interplay between different physical channels. Specifically, we examine the contributions of two main channels: RR and DR. The angular distribution of the emitted photons in these processes provides key insights into the nature of the intermediate states and the interactions that shape the emission pattern.

In this paper, we conduct a rigorous QED analysis of the angular distribution of photons emitted in two-photon electron capture by uranium ions. We explore how the photon angular emission patterns differ between the RR and DR

channels. In particular, we demonstrate that the DR channel significantly alters the angular correlation between the emitted photons. This work represents comprehensive studies of two-photon angular distributions in highly charged ions, and it highlights the importance of considering angular correlations when studying photon emission processes.

This paper is organized as follows. In Sec. II, we briefly outline the theoretical framework used to describe two-photon electron capture by H-like ions, with a more detailed description of the calculation approach given in our previous work [4]. Section III presents the energy spectrum of the emitted photons, explaining which regions of the spectrum were chosen for the analysis of the angular distribution. In Sec. IV, we present and analyze the calculated angular distribution of photons for resonant two-photon capture. We explore the one-photon angular distribution for each photon (with the angular variables of the other photon integrated out) and the two-photon angular distribution. The two-photon angular distribution is examined for two specific geometries: (1) one in which the momenta of the emitted photons are perpendicular to the momentum of the incident electron (XY plane) and (2) one in which the momenta of both photons and the incident electron lie within the same plane (XZ plane).

Relativistic units are used throughout unless otherwise stated.

II. METHOD OF CALCULATION

We perform a calculation of the differential cross section of the two-photon electron capture by a one-electron ion. The considered process is schematically described as

$$e^-(\varepsilon) + \mathrm{U}^{91+}(1s) \to \cdots \to \mathrm{U}^{90+}(1s)^2 + \gamma + \gamma', \quad (1)$$

where the initial state is the incident electron with energy ε and the one-electron ion in the ground $1s$ state. The final state is the two-electron ion in the ground $(1s)^2$ state and two emitted photons. Special attention is paid to the energy region of the emitted photons where the electron capture proceeds through the formation of one of the singly excited states. In this case, the process can be described as

$$\begin{aligned} e^-(\varepsilon) + \mathrm{U}^{91+}(1s) &\to \mathrm{U}^{90+}(1s,\, nl) + \gamma \\ &\downarrow \\ &\mathrm{U}^{90+}(1s)^2 + \gamma + \gamma'. \end{aligned} \quad (2)$$

In the DR channel, this process proceeds through the additional formation of a doubly excited state

$$\begin{aligned} e^-(\varepsilon) + \mathrm{U}^{91+}(1s) \to\ & \mathrm{U}^{90+}(nl, n'l') \to \mathrm{U}^{90+}(1s, n''l'') + \gamma \\ &\downarrow \\ &\mathrm{U}^{90+}(1s)^2 + \gamma + \gamma', \end{aligned} \quad (3)$$

where $n, n', n'' \geqslant 2$. The two-photon electron capture process (1), including its subprocesses given by (2) and (3), is treated uniformly as a composite process.

The calculation method for two-photon electron capture within QED theory was presented in a previous work [4]. Here, we focus only on the key aspects of that method. The cross section for two-photon electron capture was calculated using the line-profile approach (LPA), with a detailed description of LPA provided in [17]. In [4], this method was further generalized to accommodate two-photon electron capture.

The two-electron wave functions of the final $(1s)^2$ state and all the intermediate states in the zero-order perturbation theory are expressed in the $j-j$ coupling scheme

$$\begin{aligned} &\Psi^{(0)}_{JMn_1j_1l_1n_2j_2l_2}(\boldsymbol{r}_1, \boldsymbol{r}_2) \\ &\quad = N \sum_{m_1m_2} C^{JM}_{j_1m_1j_2m_2} \det\{\psi_{n_1j_1l_1m_1}(\boldsymbol{r}_1), \psi_{n_2j_2l_2m_2}(\boldsymbol{r}_2)\}, \end{aligned} \quad (4)$$

where the one-electron wave functions ψ_{njlm} are solutions of the Dirac equation with quantum numbers n, j, l, and m, representing the principal quantum number (or the energy for continuum electrons), total angular momentum, orbital angular momentum of the upper component, and the projection of the total angular momentum, respectively. In this expression, J and M represent the total angular momentum of the two-electron configuration and its projection, while N is the normalization constant, equal to $1/\sqrt{2}$ for nonequivalent electrons and $1/2$ for equivalent electrons. The symbols $C^{JM}_{j_1m_1j_2m_2}$ are the Clebsch-Gordan coefficients [18].

The initial state of the electron system [$1s$ and $e^-(\varepsilon)$] includes the incident electron with a certain momentum $\boldsymbol{p}$ and polarization μ (in the asymptotic $r \to \infty$). Its wave function can be written as

$$\Psi^{(0)}_{njlm,\boldsymbol{p}\mu}(\boldsymbol{r}_1, \boldsymbol{r}_2) = \frac{1}{\sqrt{2}} \det\{\psi_{njlm}(\boldsymbol{r}_1), \psi_{\boldsymbol{p}\mu}(\boldsymbol{r}_2)\}, \quad (5)$$

where ψ_{njlm} is the wave function of the bound electron and $\psi_{\boldsymbol{p}\mu}$ is the wave function of the continuum electron.

The interaction between electrons plays a crucial role in the formation of doubly excited (autoionizing) states and must therefore be properly accounted for. These doubly excited states are typically quasidegenerate, so quasidegenerate QED perturbation theory should be applied to accurately describe the DR channel.

For this purpose, we use the LPA. Within the framework of the LPA, the function describing a two-electron state, which accounts for the interaction of quantized electromagnetic and electron-positron fields, takes the following form [4,17,19]:

$$\Phi_K = \sum_N B_{NK} \Psi^{(0)}_N, \quad (6)$$

where $K \equiv (JMj_1j_2l_1l_2n_1n_2)$ is a composite index representing the complete set of quantum numbers describing the reference state K and the index N runs over all two-electron configurations, including integration over both positive- and negative-energy continua.

The coefficients B_{NK} for $N \neq K$ in Eq. (6) characterize the correlation (or mixing) between states N and K. This correlation is primarily governed by the interelectron interactions. Specifically, the correlation between the initial state and autoionizing states results in the emergence of the DR channel. The role of DR becomes more pronounced in lighter ions, as the relative contribution of the interelectron interactions increases in these systems. However, the effects resulting from the interference between RR and DR channels for the main DR resonances are more pronounced in the heavier highly charged ions [4].

In this work, for states K, where both electrons are bound, we restrict the summation over N to a basis set composed of states $(n_1 l_1, n_2 l_2)$, where $n_1 \leqslant 3$, $n_2 \leqslant 5$, and $l_1(l_2) =\leqslant 3$. For the uranium ion, this basis ensures good accuracy for states K with $n_1, n_2 \leqslant 2$ [4]. For a description of the initial state, where the incident electron is presented, we add to the basis set $(nl, e_{\mathbf{p}\mu})$ states, where $n \leqslant 3$ and $e_{\mathbf{p}\mu}$ denotes an incident electron with certain momentum and polarization. The functions Φ_K account for the electron self-energy corrections, vacuum-polarization corrections, and one- and two-photon exchange corrections. The real part of the electron self-energy correction was included using a model operator approach [20]. The imaginary part of the electron self-energy corrections, the vacuum-polarization corrections and one- and two-photon exchange corrections were accounted for through direct calculations.

Within the LPA the amplitude of the two-photon electron capture can be expressed as [17]

$$U_{FI} = \sum_N \frac{(A^{(k_1,\lambda_1)*})_{FN}(A^{(k_2,\lambda_2)*})_{NI}}{E_F + \omega_1 - E_N + \frac{i}{2}\Gamma_N} + \sum_N \frac{(A^{(k_2,\lambda_2)*})_{FN}(A^{(k_1,\lambda_1)*})_{NI}}{E_F + \omega_2 - E_N + \frac{i}{2}\Gamma_N}, \tag{7}$$

where indices I, N, and F denote the initial, intermediate, and final two-electron states with energies E_I, E_N, and E_F, respectively. The width of an intermediate state is represented by Γ_N. The two-electron matrix element of the photon emission $(A^{(k,\lambda)*})_{UD}$ reads

$$(A^{(k,\lambda)*})_{UD} = e \int d^3\mathbf{r}_1 d^3\mathbf{r}_2\, \overline{\Phi}_U(\mathbf{r}_1, \mathbf{r}_2) \times \left[\gamma^{(1)\nu} A_\nu^{(k,\lambda)*}(\boldsymbol{r}_1) + \gamma^{(2)\nu} A_\nu^{(k,\lambda)*}(\boldsymbol{r}_2)\right] \times \Phi_D(\mathbf{r}_1, \mathbf{r}_2). \tag{8}$$

In Eq. (8) $\gamma^{(i)\nu}$ are the Dirac γ matrices that act on the one-electron wave function of the argument $\boldsymbol{r}_i$. The photon wave function $A^{(k,\lambda)\nu} = (A_0^{(k,\lambda)}, \boldsymbol{A}^{(k,\lambda)})$ in the transverse gauge reads

$$A_0^{(k,\lambda)}(\boldsymbol{r}) = 0, \quad \boldsymbol{A}^{(k,\lambda)}(\boldsymbol{r}) = \sqrt{\frac{2\pi}{\omega}} e^{i\boldsymbol{k}\boldsymbol{r}} \boldsymbol{e}^{(\lambda)}, \tag{9}$$

where $\boldsymbol{k}$ is the photon wave vector, $\omega = |\boldsymbol{k}|$ is the photon energy (frequency), and $\boldsymbol{e}^{(\lambda)}$ is the polarization vector.

The fully differential cross section is connected to the amplitude as

$$\frac{d^4\sigma}{d\omega_1 d\Omega_1 d\omega_2 d\Omega_2} = \delta(\omega_1 + \omega_2 - E_I + E_F) \times |U_{FI}|^2 \frac{\varepsilon}{p} \frac{\omega_1^2 \omega_2^2}{(2\pi)^5}, \tag{10}$$

where $\Omega_{1,2}$ are the solid angles of the emitted photons.

In this work we consider unpolarized electrons and photons, which means that averaging over the incident electron polarizations μ and the polarization of the initially bound electron m_b as well as summation over photon polarizations λ_1 and λ_2 should be performed:

$$\frac{d^3\sigma}{d\omega_1 d\Omega_1 d\Omega_2} = \frac{1}{4} \sum_{\mu, m_b} \sum_{\lambda_1, \lambda_2} \int d\omega_2 \frac{d^4\sigma}{d\omega_1 d\Omega_1 d\omega_2 d\Omega_2}. \tag{11}$$

The summation in Eq. (7) runs over the complete basis set, which is constructed from the two-electron functions (6). However, to achieve good accuracy in the cross section, it is sufficient to include only intermediate singly excited $(1s, nl)$ states and $(1s, e)$ states, where one electron is in the continuum. These states directly contribute to the two primary channels: the cascade channel and the channel involving bremsstrahlung. All other states contribute significantly only to the noncascade channel, which has a minor impact within the photon energy range considered in this work (see [4]). Nevertheless, to further enhance accuracy, we also include $(2l, nl')$ states in the summation of Eq. (7). This summation is performed using a finite basis set for the Dirac equation, constructed from B splines [21,22].

III. ENERGY DISTRIBUTION

We investigate the process of electron capture by a hydrogenlike uranium ion initially in the $1s$ state, accompanied by two-photon emission. Uranium ions are chosen for this study due to the extensive theoretical research on DR in uranium, as well as the availability of experimental data (e.g., see [8,9,11]). Moreover, in uranium ions with a high nuclear charge, the interference between RR and DR is particularly pronounced, as highlighted in our previous work [4] and further explored in this study. We also note that this research builds on our previous investigation into the photon energy distribution in two-photon electron capture with uranium ions.

The incident electron energy is chosen so that the energy of the initial state $[E_I = \epsilon(e) + \epsilon(1s)]$ is close to the energy of one of the doubly excited states [such as $(2s2s)$, $(2s2p)$, and $(2p2p)$]. In this scenario, dielectronic recombination plays a significant role. Specifically, electron capture can occur through the formation of doubly excited states, followed by their subsequent decay.

The singly differential cross section of the electron capture with emission of the two photons is given by

$$\frac{d\sigma}{d\omega_1} = \int d\Omega_1 d\Omega_2 \frac{d^3\sigma}{d\omega_1 d\Omega_1 d\Omega_2}. \tag{12}$$

The energies of the emitted photons lie in the interval determined by the energy conservation law:

$$\omega_1 + \omega_2 = E_I - E_F. \tag{13}$$

Accordingly, the photon energy spectrum is continuous and limited by the energy interval $[0, \omega_{\max}]$, where $\omega_{\max} = E_I - E_F$. We note that if one of the photons is registered, then the energy of the other is determined by Eq. (13).

The total cross section reads

$$\sigma = \int_0^{\frac{\omega_{\max}}{2}} d\omega_1 \frac{d\sigma}{d\omega_1}. \tag{14}$$

In Fig. 1 we present the total cross section of two-photon electron capture as a function of incident electron kinetic energy.

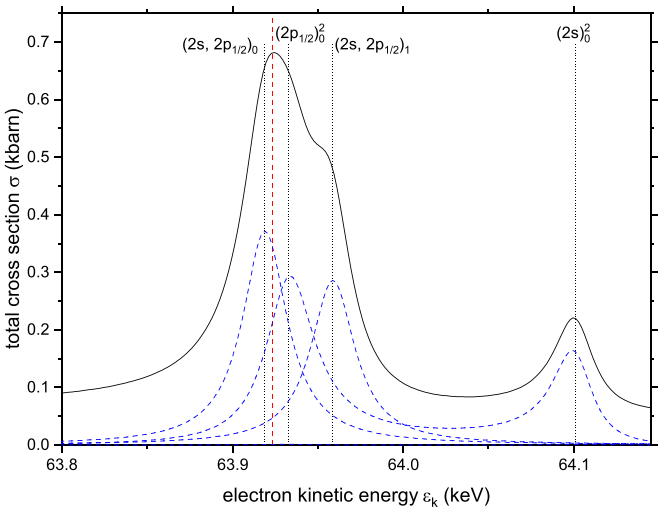

FIG. 1. Total cross section of two-photon electron capture by H-like uranium ions as a function of incident electron kinetic energy.

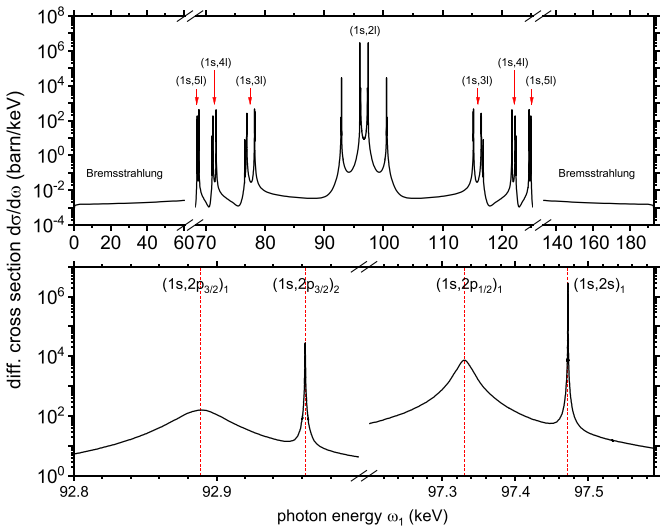

FIG. 2. Differential cross section of two-photon electron capture by H-like uranium ions as a function of the photon energy ω_1 of one of the emitted photons (the other photon energy is $\omega_2 = \omega_{\max} - \omega_1$). The kinetic energy of the incident electron equals 63.9235 keV. The red dashed lines in the bottom panel mark the positions of the cascade resonances with $(1s2l)$ states (see Table I).

The resonances in the cross section indicate a strong contribution from dielectronic recombination, manifesting in the formation of the $(2s2p_{1/2})_0$, $(2p_{1/2})^2$, $(2s2p_{1/2})_1$, and $(2s)^2$ autoionizing states. The contributions from these autoionizing states are represented by blue dashed lines. A detailed study of the total cross section of this process can be found in [4,7,10,11,19]. For further investigation of the differential cross section we choose an electron kinetic energy equal to 63.9235 keV, corresponding to the maximum of the total cross section. This energy is marked by the red dashed vertical line in Fig. 1. For this collision energy, Eq. (13) has the form

$$\omega_1 + \omega_2 = 193.4885\,\text{keV}. \tag{15}$$

In Fig. 2, we present a differential cross section of two-photon electron capture as a function of energy for one of the emitted photons for a chosen incident electron kinetic energy. A detailed investigation of the photon energy distribution was performed in our previous work [4]. Since the two-photon states $(\boldsymbol{k}_1, \lambda_1; \boldsymbol{k}_2, \lambda_2)$ and $(\boldsymbol{k}_2, \lambda_2; \boldsymbol{k}_1, \lambda_1)$ are identical, the differential cross section (12) is symmetric with respect to the center of the energy interval $[0, \omega_{\max}]$. The two-photon electron capture predominantly proceeds via cascade transitions $(1s, e) \to (1s, nl) \to (1s)^2$ with the formation of singly excited $(1s, nl)$ states with $n \geqslant 2$. In particular, the main contributions come from the energy regions corresponding to the cascade transitions through the $(1s2s)$ and $(1s2p)$ states. Therefore, we focus on the four pairs of photon energies $(\omega_1^{\text{res},N}, \omega_2^{\text{res},N})$, which are associated with the formation and radiative decay of four singly excited states N: $(1s2s)_1$, $(1s2p_{1/2})_1$, $(1s2p_{3/2})_1$, and $(1s2p_{3/2})_2$. These energies are presented in Table I and are shown by the vertical red dashed lines in the bottom panel of Fig. 2.

TABLE I. The cascade energies of the emitted photons $\omega_1^{\text{res},N} = E_I - E_N$ and $\omega_2^{\text{res},N} = E_N - E_F$ and the natural linewidths Γ_N of the corresponding singly excited states.

State N	$\omega_1^{\text{res},N}$ (keV)	$\omega_2^{\text{res},N}$ (keV)	Γ_N (eV)
$(1s2s)_1$	97.4668	96.0217	0.09
$(1s2p_{1/2})_1$	97.3257	96.1628	20.3
$(1s2p_{3/2})_1$	92.8835	100.605	34.0
$(1s2p_{3/2})_2$	92.9572	100.5313	0.22

We note that intermediate singly excited states with zero total angular momentum [such as $(1s2s)_0$ and $(1s2p_{1/2})_0$] do not appear in the spectrum of two-photon electron capture. To take into account cascade resonances involving these states, it is necessary to consider electron capture involving the emission of three or more photons.

The energies listed in Table I are calculated with an accuracy of 0.5 eV. The width of the $(1s2s)_1$ state is determined with an accuracy of about 5%, while the widths of the other states are calculated with a higher accuracy of better than 2%. The overall accuracy of the cross-section calculations varies depending on the photon energy range and is estimated to be better than 5%.

Strictly speaking, in a two-photon process, we cannot assign a specific photon to the particular transition. However, the two photons can be distinguished by their energies. In the bottom panel of Fig. 2, we consider photon energy regions that include the energy differences between the initial state and singly excited states $(E_I - E_{(1s2l)})$. The energy of the other photon (determined by the energy conservation law) is close to the energy difference between a singly excited state and the final state $(E_{(1s2l)} - E_F)$. These two photons are therefore distinguishable by their energies. We refer to the first photon $(\omega_1, \boldsymbol{k}_1)$ as the resonant photon, with an energy corresponding to the $(1s, e) \to (1s, 2l)$ transition, and the second photon $(\omega_2, \boldsymbol{k}_2)$ as the satellite photon, with an energy corresponding to the $(1s, 2l) \to (1s, 1s)$ transition.

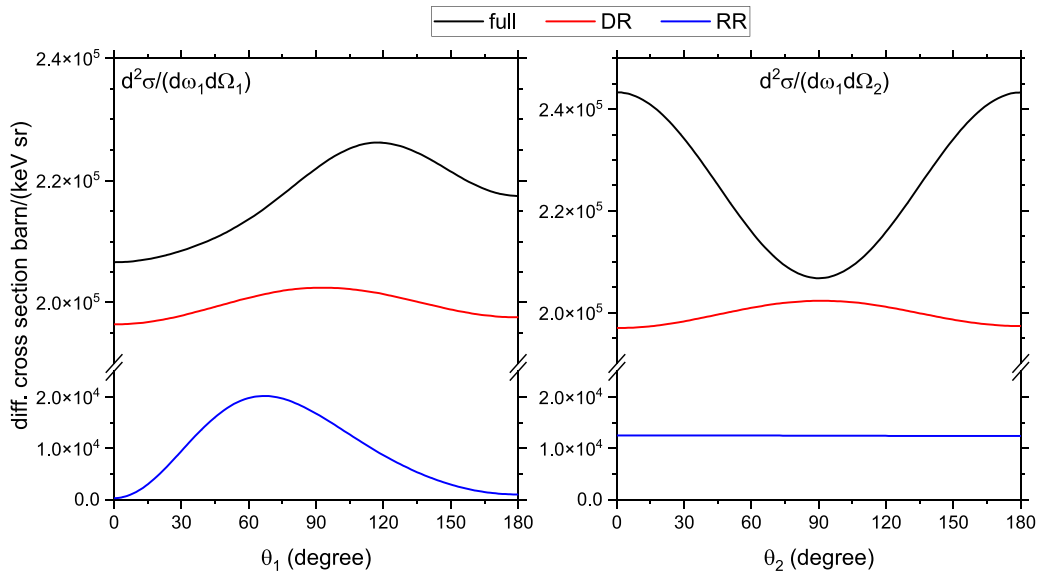

FIG. 3. Differential cross section as a function of the polar angle of one of the emitted photons (θ_1 or θ_2). The photon energy corresponds to $(1s2s)_1$ cascade resonance. The left panel corresponds to the first photon with energy $\omega_1 = E_I - E_{(1s2s)_1} = 97.4668$ keV, and the right panel corresponds to the second photon with energy $\omega_2 = E_{(1s2s)_1} - E_F = 96.0217$ keV. The black curve shows the result of the full calculation, the red curve corresponds to the DR contribution, and the blue curve demonstrates the RR contribution.

IV. ANGULAR DISTRIBUTION

We align the z axis with the momentum of the incident electron and measure the polar angle θ from this axis. The photon momentum is described by the photon energy ω, the polar angle θ, and the azimuthal angle φ: $\boldsymbol{k} = \boldsymbol{k}(\omega, \theta, \varphi)$. The differential cross section for two-photon ($\boldsymbol{k}_1$ and $\boldsymbol{k}_2$) emission is characterized by the angles of both photons. However, because of the presence of axial symmetry, the differential cross section depends only on the difference in the azimuthal angles:

$$\frac{d^3\sigma}{d\omega_1 d\Omega_1 d\Omega_2} = \frac{d^3\sigma}{d\omega_1 d\Omega_1 d\Omega_2}(\omega_1, \theta_1, \theta_2, |\varphi_2 - \varphi_1|). \quad (16)$$

It is worth noting that, due to the identity of the two pairs $(\boldsymbol{k}_1, \boldsymbol{k}_2)$ and $(\boldsymbol{k}_2, \boldsymbol{k}_1)$ of emitted photons, the following equality holds:

$$\frac{d^3\sigma}{d\omega_1 d\Omega_1 d\Omega_2}(\omega_1, \theta_1, \theta_2, |\varphi_2 - \varphi_1|) = \frac{d^3\sigma}{d\omega_1 d\Omega_1 d\Omega_2}(\omega_{\max} - \omega_1, \theta_2, \theta_1, |\varphi_2 - \varphi_1|). \quad (17)$$

A. One-photon angular distribution

Here, we assume that only one [either $(\omega_1, \boldsymbol{k}_1)$ or $(\omega_2, \boldsymbol{k}_2)$] of the emitted photons is detected. Accordingly, to investigate the one-photon angular distribution, we consider the differential cross section in which integration over the angular variables of the first or second emitted photons is performed,

$$\frac{d^2\sigma}{d\omega_1 d\Omega_1} = \int d\Omega_2 \frac{d^3\sigma}{d\omega_1 d\Omega_1 d\Omega_2}, \quad (18)$$

$$\frac{d^2\sigma}{d\omega_1 d\Omega_2} = \int d\Omega_1 \frac{d^3\sigma}{d\omega_1 d\Omega_1 d\Omega_2}, \quad (19)$$

respectively. We note that these differential cross sections are independent of the azimuthal photon angles φ_i. The differential cross sections as function of the polar angle θ_i of the first or second emitted photon are presented in Figs. 3–6, where the photon energies are $\omega_1 = E_I - E_N$ and $\omega_2 = E_N - E_F$, with N representing one of the $(1s2s)_1$, $(1s2p_{1/2})_1$, $(1s2p_{3/2})_1$, and $(1s2p_{3/2})_2$ states, respectively. The contributions from the DR and RR channels are shown separately. The DR channel is dominant for the $(1s2s)_1$ and $(1s2p_{1/2})_1$ cascades (Figs. 3 and 4), while the RR channel is dominant for the $(1s2p_{3/2})_{1,2}$ cascades (Figs. 5 and 6). We observe that the significant contribution from the DR channel results in the differential cross section for the DR resonances being substantially larger than that for the RR resonances. Figures 3–6 indicate that the shape of the angular distribution depends on the relative contributions of the RR and DR channels. In the RR channel, the first photon is typically emitted in the forward direction, regardless of the resonance. In contrast, in the DR channel, the angular distribution of the first emitted photon can vary significantly depending on the specific autoionizing state formed. The second photon in both channels has a symmetrical distribution with respect to 90°.

Figures 3–6 also show evidence of strong interference between the RR and DR channels. The cascade contribution of the second photon is associated with the $(1s2l) \to (1s1s)$ transitions in both channels. The corresponding RR and DR amplitudes differ only by a phase shift, leading to significant interference in transitions where both the RR and DR channels are strong. For the first photon, the situation is different: In the RR channel, the cascade contribution comes from the $(1s, e) \to (1s, 2l)$ transition, while in the DR channel, it originates from the $(2s2p) \to (1s2l)$ transition. Since the corresponding RR and DR amplitudes are substantially different, the interference between the RR and DR channels for the first photon is less pronounced.

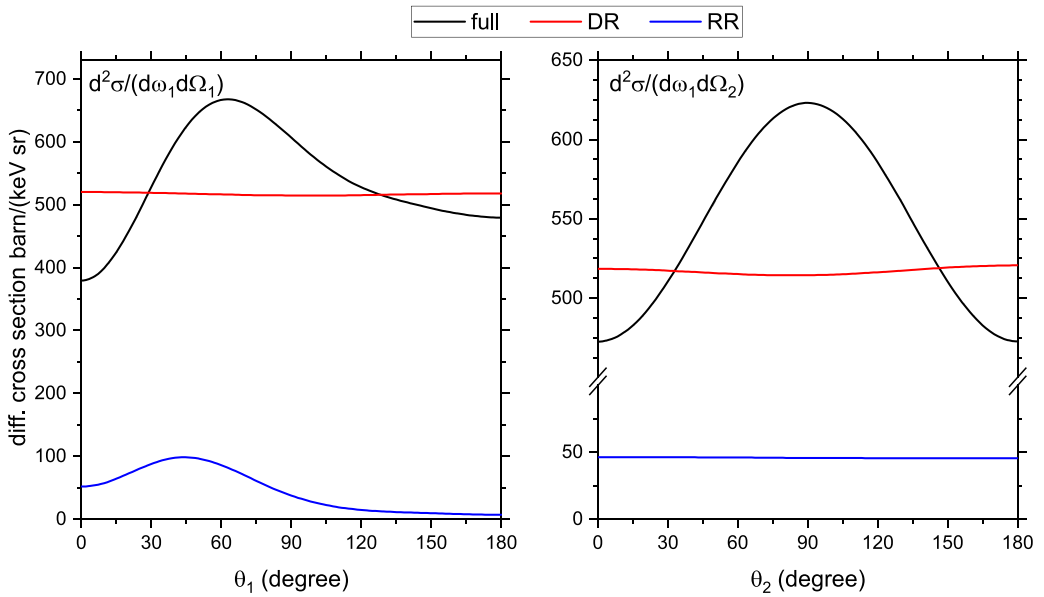

FIG. 4. The same as in Fig. 3, but for photon energy corresponding to $(1s2p_{1/2})_1$ cascade resonance: $\omega_1 = 97.3257$ keV and $\omega_2 = 96.1628$ keV.

To account for the accuracy of the photon detectors and the energy spread of the incident electrons in the beam, we perform integration over the energy of the emitted photons. The four considered cascade resonances can be divided into two groups of resonances that are close in energy. The first group includes cascade transitions with the formation of the $(1s2s)_1$ and $(1s2p_{1/2})_1$ states, while the second group includes cascades transitions with the formation of the $(1s2p_{3/2})_1$ and $(1s2p_{3/2})_2$ states. The integration energy interval is $[\omega_1^{(\mathrm{res},N)} - 50\Gamma_N, \omega_1^{(\mathrm{res},N)} + 50\Gamma_N]$, where $N = (1s2p_{1/2})_1$ for the first group and $N = (1s2p_{3/2})_1$ for the second group. The energies $\omega_1^{(\mathrm{res},N)}$ and widths Γ_N are presented in Table I. The results of these integrations are given in Fig. 7. This figure shows that after integration over the energy intervals, the first photon still has a noticeable maximum in the angular distribution and tends to be emitted in the forward direction, while the second photon exhibits almost isotropic behavior for both groups of resonances. The reason for the isotropic behavior is the significant compensation of the maximum of the angular distribution for one resonance and the minimum for the other in each group. We note that in each resonance group, one of the resonances has a small maximum in the energy differentiated cross section but has a large width, and the other, on the contrary, has a large energy differentiated cross section and

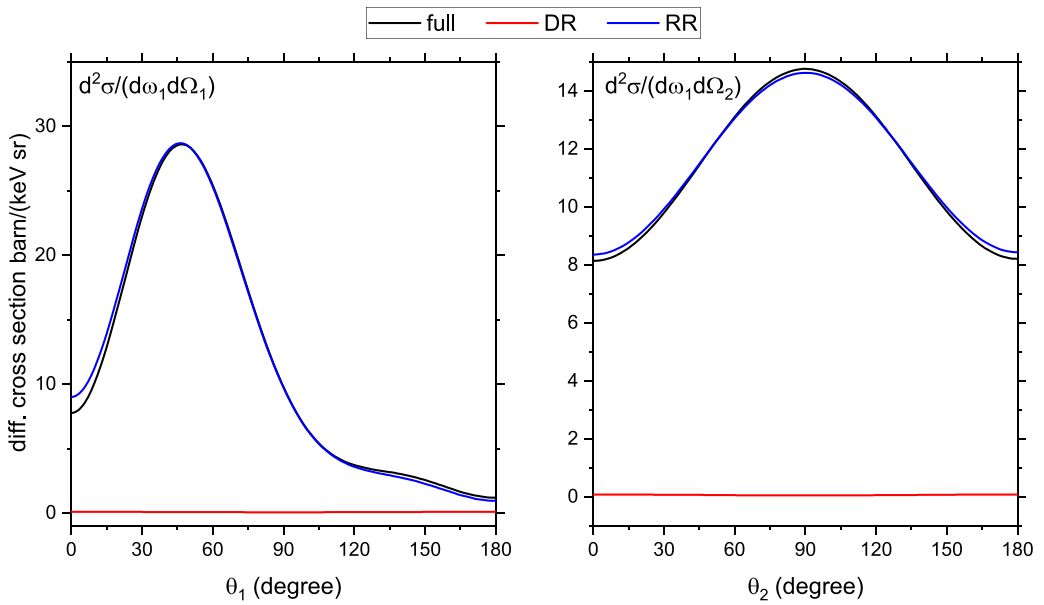

FIG. 5. The same as in Fig. 3, but for photon energy corresponding to $(1s2p_{3/2})_1$ cascade resonance: $\omega_1 = 92.8835$ keV and $\omega_2 = 100.605$ keV.

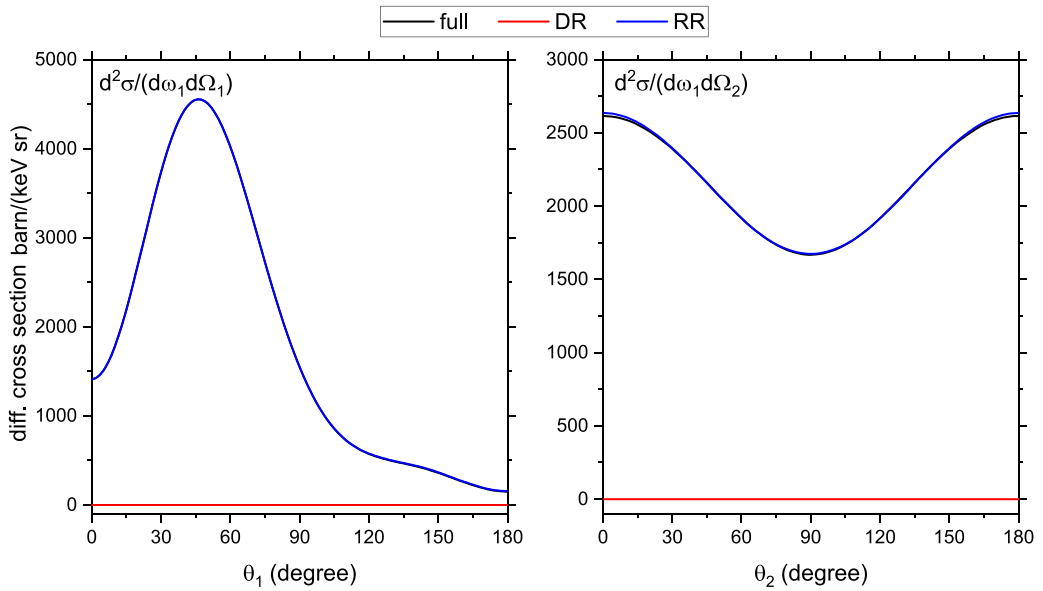

FIG. 6. The same as in Fig. 3, but for photon energy corresponding to $(1s2p_{3/2})_2$ cascade resonance: $\omega_1 = 92.9572$ keV and $\omega_2 = 100.5313$ keV.

a small width, which provides compensation, leading to the isotropic distribution.

The angular distribution of the DR process within the single-photon approximation (where the angular distribution of only the first photon is available) was studied in [7,9,10]. The angular distribution of the first photon, obtained within this approximation, is shown as black dashed curves in Fig. 7. The angular distribution of the first photon in the full calculation and approximation is qualitatively similar, but there is a noticeable quantitative difference. We explain this difference as follows. First, the destructive interference between cascade resonances decreases the cross

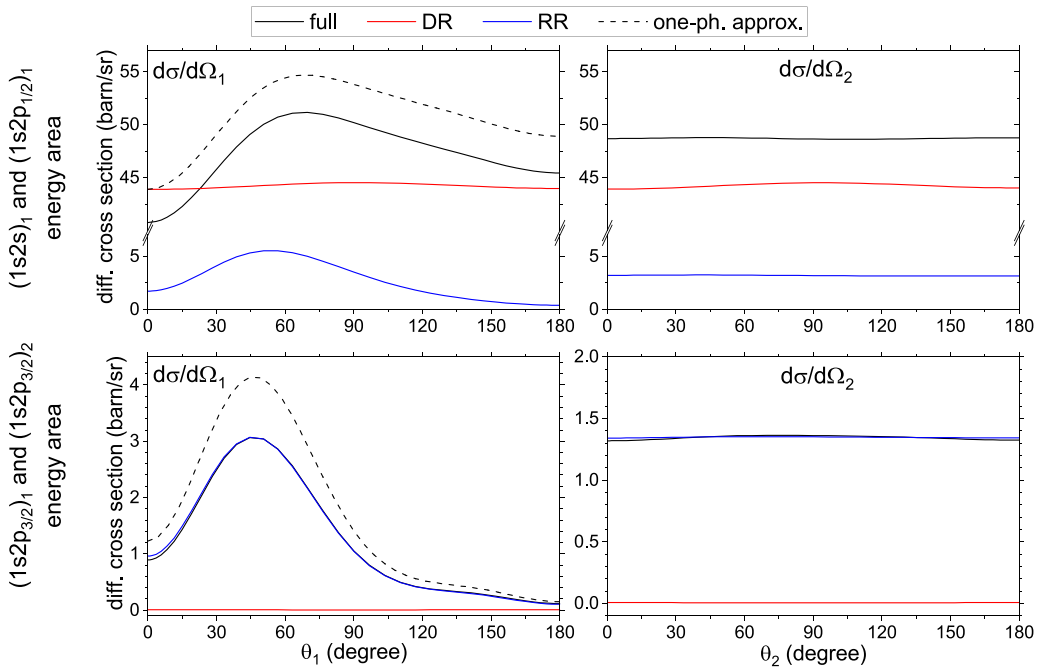

FIG. 7. The differential cross section is presented as a function of the polar angle of one of the emitted photons. The left panels show the angular distribution of the first photon (with energy $\omega_1 \approx E_I - E_{(1s2l)}$), while the right panels show the angular distribution of the second photon (with energy $\omega_2 \approx E_{(1s2l)} - E_F$). The top panels display the differential cross section after integration over the photon energy ω_1 within the [96.312, 98.339] keV interval, which includes two close cascade resonances with $(1s2s)_1$ and $(1s2p_{1/2})_1$ states. The bottom panels show the differential cross section after integration within the [91.181, 94.585] keV interval, which includes two other close cascade resonances with $(1s2p_{3/2})_1$ and $(1s2p_{3/2})_2$ states. The black curve shows the result of the full calculation, the red curve corresponds to the DR contribution, and the blue curve demonstrates the RR contribution.

section. Second, the results of the single-photon approximation are close to the results of the exact calculation if the ratio of the partial single-photon width corresponding to the decay to the ground state $\Gamma_N^{(1\gamma,N\to 1s^2)}$ to the total width Γ_N is close to unity ($\Gamma_N^{(1\gamma,N\to 1s^2)}/\Gamma_N \approx 1$) for each intermediate cascade state N (see Eq. (A8) in [4]). This ratio is, indeed, close to unity for the states $(1s2s)_1$, $(1s2p_{1/2})_1$, and $(1s2p_{3/2})_1$, but for the state $(1s2p_{3/2})_2$ this ratio is 0.62 due to the presence of the single-photon $(1s2p_{3/2})_2 \to (1s2s)_1$ transition. Finally, the third reason is the limited interval of integration.

B. Two-photon angular distribution

Here, we assume that both of the emitted photons are detected. The process is characterized by three vectors: $\boldsymbol{p} = p\boldsymbol{e}_z$, $\boldsymbol{k}_1(\theta_1, \varphi_1)$, and $\boldsymbol{k}_2(\theta_2, \varphi_2)$, so we align the z axis with the momentum of the incident electron. To study the two-photon angular distribution of the emitted photons, we select two characteristic collision geometries. In the first, the photon momenta lie in the XY plane, while in the second, they lie in the XZ plane. We believe that the data obtained from these geometries can be used to estimate distributions in other planes, offering a broader understanding of the two-photon angular distribution.

1. XY plane

In the collision geometry where both emitted photon momenta lie in the XY plane ($\theta_1 = \theta_2 = 90^\circ$), the differential cross section depends only on the angle between the photon momenta. The differential cross section $\frac{d^3\sigma}{d\omega_1 d\Omega_1 d\Omega_2}$ can be considered a function of ω_1 and $\varphi = |\varphi_2 - \varphi_1|$,

$$\frac{d^3\sigma^{XY}}{d\omega_1 d\Omega_1 d\Omega_2}(\omega_1, \varphi) = \frac{d^3\sigma}{d\omega_1 d\Omega_1 d\Omega_2}\left(\omega_1, \frac{\pi}{2}, \frac{\pi}{2}, |\varphi_2 - \varphi_1|\right). \tag{20}$$

Due to the identity of the emitted photons, the cross section has the following energy symmetry in the XY plane:

$$\frac{d^3\sigma^{XY}}{d\omega_1 d\Omega_1 d\Omega_2}(\omega_1, \varphi) = \frac{d^3\sigma^{XY}}{d\omega_1 d\Omega_1 d\Omega_2}(\omega_{\max} - \omega_1, \varphi). \tag{21}$$

The differential cross section is shown in Fig. 8. The horizontal axis represents the energy of the first photon, and the vertical axis represents the angle between photon momenta φ. We can observe the contribution of the four singly excited states $[(1s2s)_1$, $(1s2p_{1/2})_1$, $(1s2p_{3/2})_1$, and $(1s2p_{3/2})_2]$ to the angular distribution. As before, we focus on the differential cross section at fixed photon energies corresponding to the maxima of the cascade resonances marked by red lines in the bottom panel of Fig. 2 and presented in Table I.

To investigate the φ dependence in Eq. (16), it is convenient to introduce the normalized differential cross section

$$\frac{d^3\tilde{\sigma}^{XY}}{d\omega_1 d\Omega_1 d\Omega_2} = \frac{d^3\sigma^{XY}}{d\omega_1 d\Omega_1 d\Omega_2} \Big/ \frac{d^3\sigma^{XY}}{d\omega_1 d\cos\theta_1 d\cos\theta_2}, \tag{22}$$

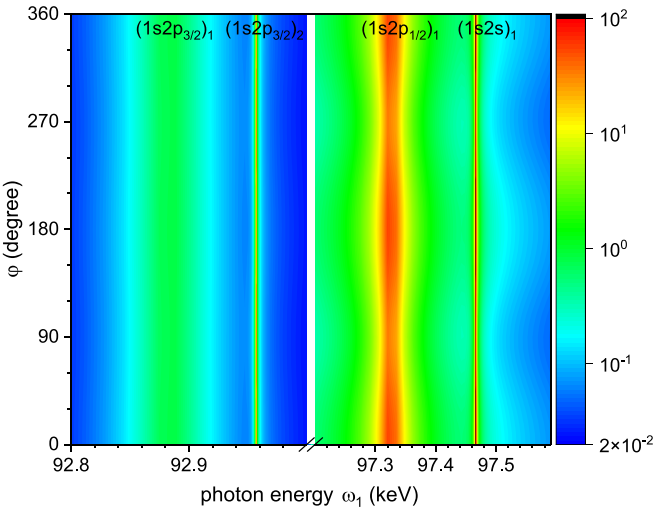

FIG. 8. XY plane. Differential cross section [in barn/(keV sr^2)] for two-photon electron capture by a H-like uranium ion, shown as a function of the energy of the first photon ω_1 and the angle between photons momenta φ. The narrow vertical black region, located at the $(1s2s)_1$ resonance, represents a differential cross section exceeding 100 barn/(keV sr^2), with a maximum value of 2.4×10^4 barn/(keV sr^2).

where

$$\frac{d^3\sigma^{XY}}{d\omega_1 d\cos\theta_1 d\cos\theta_2} = \int \frac{d^3\sigma^{XY}}{d\omega_1 d\Omega_1 d\Omega_2} d\varphi_1 d\varphi_2. \tag{23}$$

In Fig. 9, we present the normalized differential cross section (22) for the photon energies corresponding to the four cascade resonances under consideration. The dependence on φ can be factorized and parameterized quite accurately as follows:

$$\frac{d^3\tilde{\sigma}^{XY}}{d\omega_1 d\Omega_1 d\Omega_2} \approx \frac{1}{2\pi}[C(\omega_1) - A(\omega_1)\sin^2\varphi]. \tag{24}$$

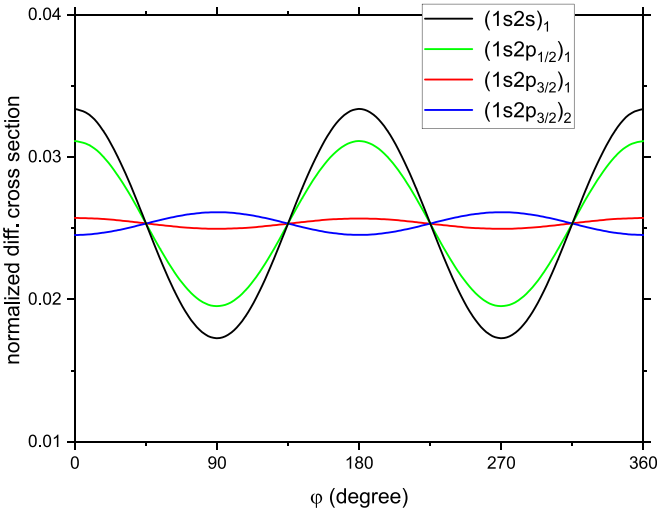

FIG. 9. XY plane. Normalized differential cross section of the two-photon electron capture by H-like uranium ions as a function of $\varphi = |\varphi_2 - \varphi_1|$ for photon energies corresponding to $(1s2l)$ cascade resonances (see Table I).

TABLE II. Parameters of the approximation (24) of the differential cross section with fixed polar angles of the photon momenta ($\theta_1 = \theta_2 = \pi/2$).

State	$\frac{d^3\sigma^{XZ}}{d\omega_1 d\cos\theta_1 d\cos\theta_2}$ (barn/keV)	C (10^{-2} rad^{-2})	A (10^{-2} rad^{-2})
$(1s2s)_1$	7.04×10^5	3.34	1.61
$(1s2p_{1/2})_1$	2.28×10^3	3.11	1.16
$(1s2p_{3/2})_1$	35.4	2.57	0.076
$(1s2p_{3/2})_2$	4.15×10^3	2.45	−0.16

The normalization condition yields the following relation between A and C: $\pi(2C - A) = 1$. The values of C and A are listed in Table II. The unpolarized cross section $\frac{d^3\tilde{\sigma}^{XY}}{d\omega_1 d\Omega_1 d\Omega_2}$ as a function of φ has a symmetrical shape relative to the center of $[0, 2\pi]$. We note that, for fixed photon and electron polarizations, Eq. (20) does not take place, and this symmetry is absent.

From Fig. 9, we observe that the differential cross sections for the $(1s2s)_1$ and $(1s2p_{1/2})_1$ cascades exhibit a more pronounced angular dependence compared to those for the $(1s2p_{3/2})_{1,2}$ cascades. This behavior is linked to the role of the DR channel. As discussed in Sec. IV A, the DR channel plays a significant role in the $(1s2s)_1$ and $(1s2p_{1/2})_1$ cascades, while it is strongly suppressed by the RR channel in the $(1s2p_{3/2})_{1,2}$ cascades. To clarify this phenomenon, we present the normalized contributions of the DR and RR channels separately, along with the full calculation, in Fig. 10. From Fig. 10, we can see that the DR exhibits a noticeable angular dependence, whereas the angular dependence for the RR is relatively weak. Therefore, we conclude that the significant angular dependence observed for the $(1s2s)_1$ and $(1s2p_{1/2})_1$ cascades is evidence of the DR channel's influence, while the weak angular dependence for the $(1s2p_{3/2})_{1,2}$ cascades indicates the limited role of the DR channel in these cascades.

2. *XZ plane*

Here, we consider photons with momenta in the XZ plane, so the photon momenta $\boldsymbol{k}_1$ and $\boldsymbol{k}_2$ and the incident electron momentum $\boldsymbol{p}$ lie in the same plane. Accordingly, in this collision geometry, the azimuthal angles of the emitted photons (φ_i, $i = 1, 2$) can take two values: 0° and 180°. The polar angles (θ_i, $i = 1, 2$) vary within the interval $[0, \pi]$.

It is convenient to introduce an angle $\tilde{\theta}_i$ varying within the interval $[0, 2\pi]$:

$$\tilde{\theta}_i = \begin{cases} \theta_i & \text{for} \quad \varphi_i = 0°, \\ 2\pi - \theta_i & \text{for} \quad \varphi_i = 180°. \end{cases} \tag{25}$$

We investigate the differential cross section as a function of ω_1, $\tilde{\theta}_1$, and $\tilde{\theta}_2$:

$$\frac{d^3\sigma^{XZ}}{d\omega_1 d\Omega_1 d\Omega_2}(\omega_1, \tilde{\theta}_1, \tilde{\theta}_2) = \frac{d^3\sigma}{d\omega_1 d\Omega_1 d\Omega_2}(\omega_1, \theta_1, \theta_2, |\varphi_2 - \varphi_1|), \tag{26}$$

where $\tilde{\theta}_i$ is related to θ_i and φ_i in accordance with Eq. (25).

In Fig. 11, we present the angular differential cross section for the emitted photons corresponding to the four cascade

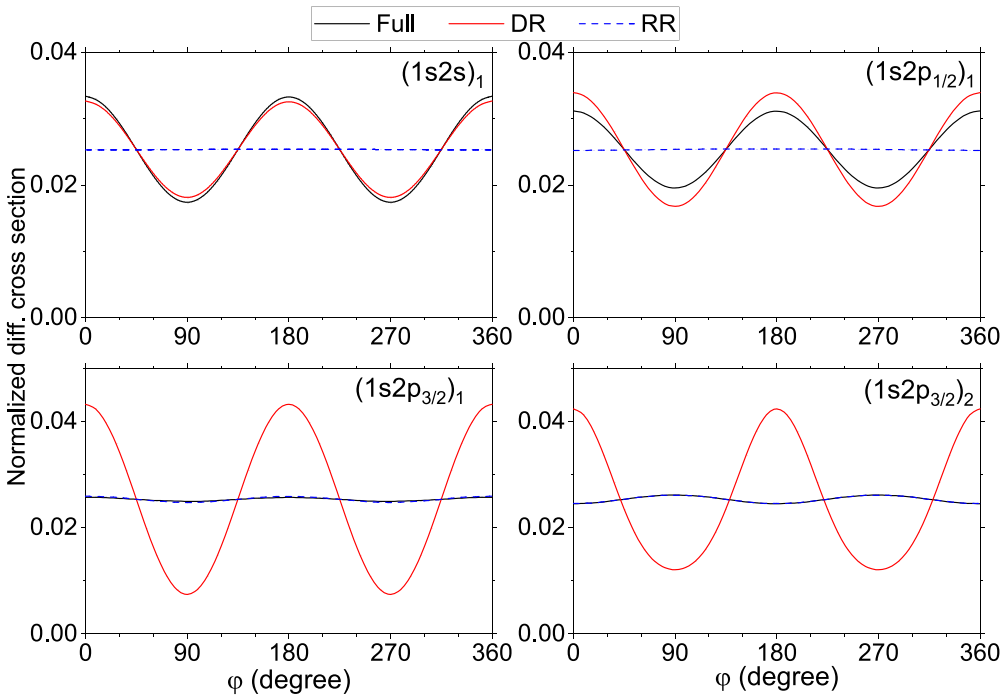

FIG. 10. XY plane. Normalized differential cross section of the two-photon electron capture by H-like uranium ions as a function of $\varphi = |\varphi_2 - \varphi_1|$ for photon energies corresponding to $(1s2l)$ cascade resonances (see Table I). The black line corresponds to the full calculation. The blue and red lines correspond to calculations that take into account only RR and DR, respectively.

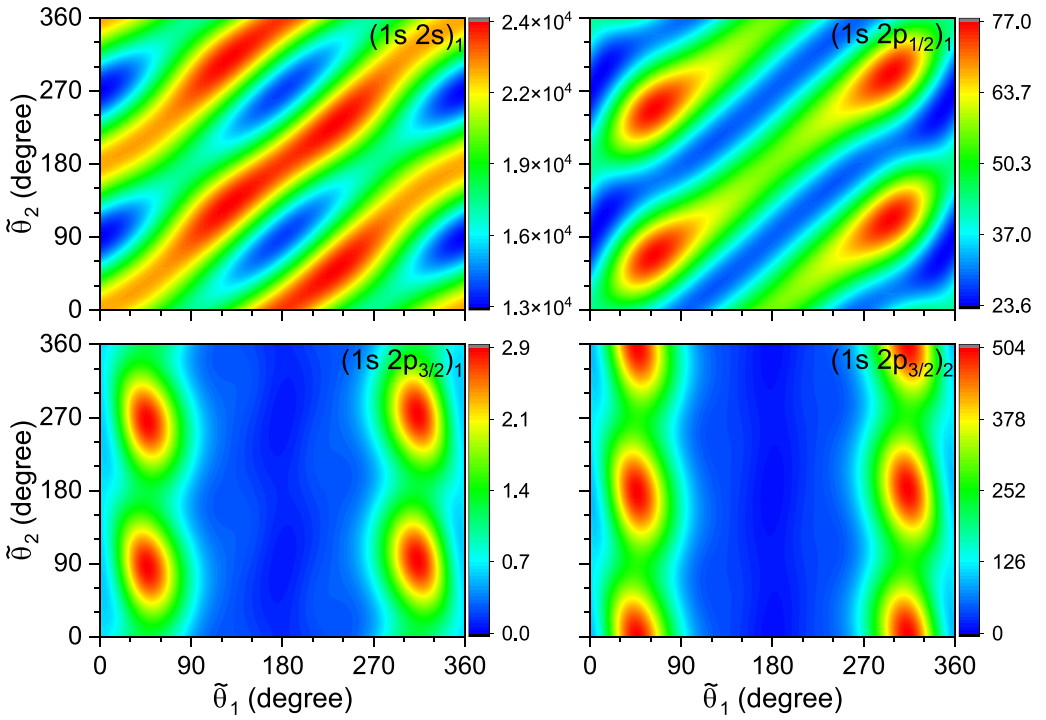

FIG. 11. XZ plane. Differential cross section of the two-photon electron capture by H-like uranium ions as a function of $\tilde{\theta}_1$ and $\tilde{\theta}_2$. The photon energies correspond to $(1s2l)$ cascade resonances (see Table I).

resonances under consideration. The energies $\omega_1^{(\mathrm{res},N)}$ associated with these resonances are shown in the Table I.

Due to the azimuthal symmetry of the process relative to the direction of the incident electron momentum, we have the following symmetry in the XZ plane:

$$\frac{d^3\sigma^{XZ}}{d\omega_1 d\Omega_1 d\Omega_2}(\omega_1, \tilde{\theta}_1, \tilde{\theta}_2) = \frac{d^3\sigma^{XZ}}{d\omega_1 d\Omega_1 d\Omega_2}(\omega_1, 2\pi - \tilde{\theta}_1, 2\pi - \tilde{\theta}_2). \quad (27)$$

The complex structure of the two-photon angular distribution is reflected in the one-photon angular distribution, as discussed in Sec. IV A. For instance, the two-photon distribution for the photon energy corresponding to the $(1s2p_{3/2})_2$ cascade shows two maxima at $\tilde{\theta}_1 = 45^\circ$ and 315° (for fixed $\tilde{\theta}_2$) and three maxima at $\tilde{\theta}_2 = 0^\circ$, 180°, and 360° (for fixed $\tilde{\theta}_1$). This pattern matches the one-photon distribution shown in Fig. 6, where θ_1 has a maximum at $\theta_1 = 45^\circ$ and θ_2 has two maxima at $\theta_2 = 0^\circ, 180^\circ$.

We observe that in cascades where the DR channel dominates $[(1s2s)_1$ and $(1s2p_{1/2})_1]$, the emitted photons are significantly more correlated than in cascades where the RR channel dominates $[(1s2p_{3/2})_1$ and $(1s2p_{3/2})_2]$. For instance, in the $(1s2s)_1$ cascade, for any given angle $\tilde{\theta}_1$, there is a corresponding $\tilde{\theta}_2$ where the differential cross section shows a pronounced maximum. In contrast, for the $(1s2p_{3/2})_1$ cascade, when $\tilde{\theta}_1 = 180$, the differential cross section remains small for all values of $\tilde{\theta}_2$.

The obtained angular distribution is shaped by the relative contributions of the DR and RR channels for each cascade resonance. In the top panels, the DR channel dominates, while in the bottom panels, the RR channel contribution is more significant. To illustrate this, we show the individual contributions of the DR and RR channels separately in Figs. 12 and 13.

In the DR-dominated cascades, when only the DR channel is considered (as shown in the top panels of Fig. 12), we find that the first photon can be emitted in any direction, but the second photon remains correlated with it. Alternatively, the second photon can be emitted in any direction, and the first photon adjusts to its direction. A similar trend is evident in the RR-dominated cascades (bottom panels of Fig. 12), although to a lesser extent, as the RR resonances are weaker and cannot be fully isolated from DR contributions.

In Fig. 13, where only the RR channel contribution is considered, we see a weak dependence on the second photon, reflecting the weak correlation between the first photon, corresponding to the transition from the initial state to the singly excited state, and the second photon, which corresponds to the transition from the singly excited state to the ground state.

V. SUMMARY

We investigated the photon angular distribution in resonant two-photon electron capture by H-like uranium. Our study focused on the incident electron energy that corresponds to the largest contribution from the DR channel and the maximum of the total cross section. We conducted a detailed analysis of the main cascade transitions $[(1s2p)$ and $(1s2s)]$, which contribute the most significantly to the cross section. We investigated the one-photon angular distribution, in which the integration over the angles of one of the photons was performed. The angular distribution of the resonant photon is in qualitatively good agreement with results obtained within the single-photon approximation. Going beyond the single-photon approximation, we examined the angular distribution of the satellite photon.

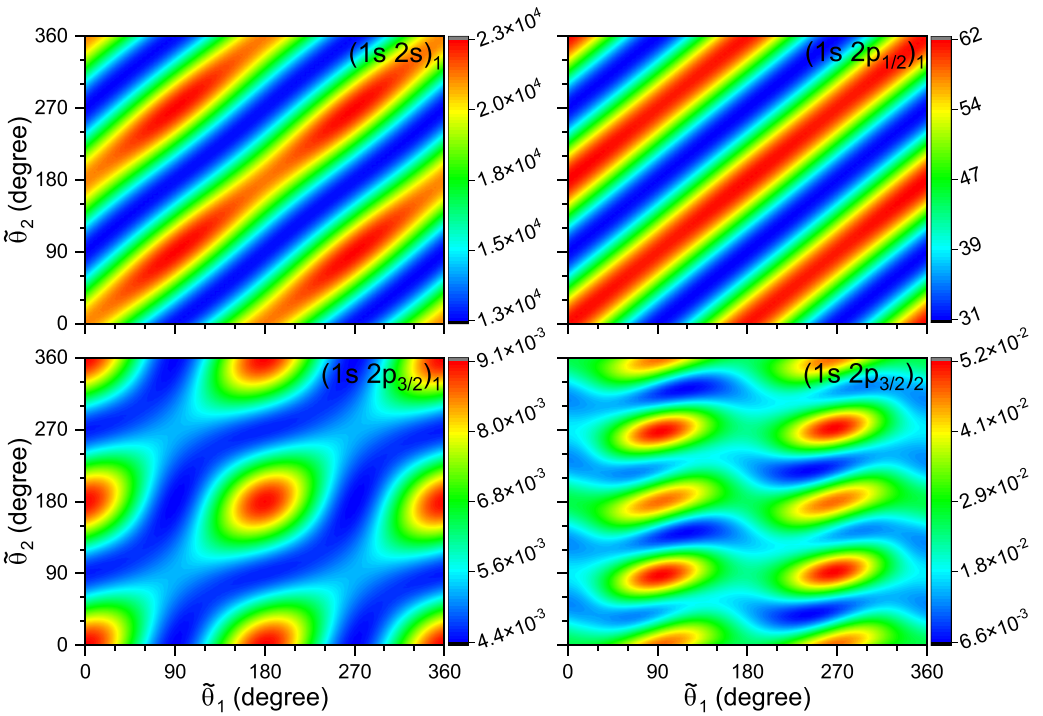

FIG. 12. XZ plane. The same as in Fig. 11, but only the DR channel is taken into account.

We analyzed the two-photon angular distribution for two specific geometries: the XY plane, where the photon momenta are perpendicular to the incident electron momentum, and the XZ plane, where the incident electron and the photon momenta lie in the same plane. The angular distribution of the photons depends on the relative contributions of the DR and RR channels. The cascade resonances considered fall into two categories: those dominated by the DR channel and those dominated by the RR channel.

In the XY plane, the DR channel exhibits noticeable oscillations in the angular distribution, while the RR channel leads to a more isotropic pattern, shaping the overall angular dependence in this plane.

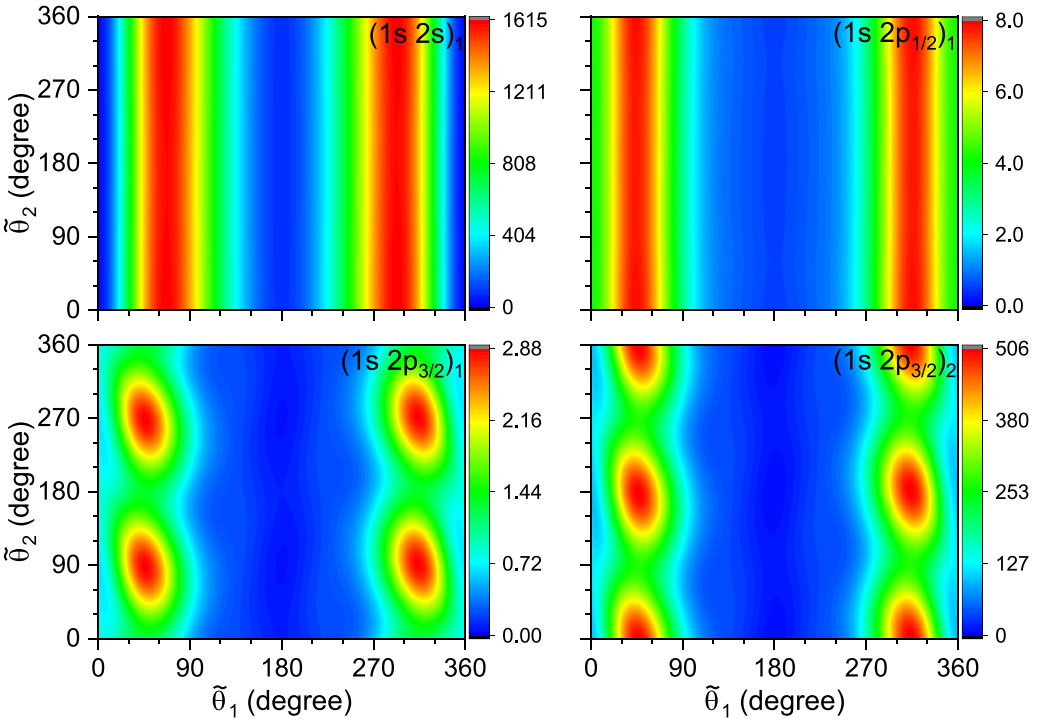

FIG. 13. XZ plane. The same as in Fig. 11, but only the RR channel is taken into account.

In the XZ plane, for the RR-dominated resonances, the photons associated with the free-bound transition are not aligned with the incident electron momentum, and the second photons show only a weak correlation with the direction of the first photons. On the contrary, for resonances dominated by the DR, the emitted photons correlate with each other, but not with the incident electron momentum.

The presented investigation of the RR and DR channels demonstrates strong interference between these channels in the two-photon angular distribution.

ACKNOWLEDGMENTS

The work of D.Y. is supported by the National Key Research and Development Program of China under Grant No. 2022YFA1602501 and the National Natural Science Foundation of China under Grant No. 12011530060. The work of K.N.L. and O.Y.A. was supported by the Chinese Academy of Sciences (CAS) Presidents International Fellowship Initiative (PIFI) under Grants No. 2022VMC0002 and No. 2025PVA0072, respectively.

[1] N. Nakamura, H. Tobiyama, H. Nohara, A. P. Kavanagh, H. Watanabe, H. A. Sakaue, Y. Li, D. Kato, F. J. Currell, C. Yamada, and S. Ohtani, Resonant electron processes with open-shell highly charged ion targets, J. Phys.: Conf. Ser. **58**, 267 (2007).

[2] Z. Yang, J. Gao, W. Yan, K. Yao, J. Yang, Z. Wu, and Z. Hu, Anisotropy and polarization of x-ray line emissions in the dielectronic recombination of hydrogenlike Fe^{25+} ions, Phys. Rev. A **104**, 022809 (2021).

[3] N. Nakamura, N. Numadate, S. Oishi, X.-M. Tong, X. Gao, D. Kato, H. Odaka, T. Takahashi, Y. Tsuzuki, Y. Uchida, H. Watanabe, S. Watanabe, and H. Yoneda, Strong polarization of a $J = 1/2$ to $1/2$ transition arising from unexpectedly large quantum interference, Phys. Rev. Lett. **130**, 113001 (2023).

[4] K. N. Lyashchenko, O. Y. Andreev, and D. Yu, Two-photon electron capture by H-like uranium, Phys. Rev. A **109**, 032805 (2024).

[5] J. Eichler and T. Stöhlker, Radiative electron capture in relativistic ion-atom collisions and the photoelectric effect in hydrogen-like high-Z systems, Phys. Rep. **439**, 1 (2007).

[6] J. Eichler, A. Ichihara, and T. Shirai, Photon angular distributions from radiative electron capture in relativistic atomic collisions, Phys. Rev. A **51**, 3027 (1995).

[7] V. Karasiov, L. Labzowsky, A. Nefiodov, and V. Shabaev, Overlapping resonances in the process of recombination of an electron with hydrogenlike uranium, Phys. Lett. A **161**, 453 (1992).

[8] M. Zimmermann, N. Grün, and W. Scheid, Photo recombination on highly charged few-electron uranium ions, J. Phys. B **30**, 5259 (1997).

[9] D. Bernhardt *et al.*, Breit interaction in dielectronic recombination of hydrogenlike uranium, Phys. Rev. A **83**, 020701(R) (2011).

[10] K. N. Lyashchenko and O. Y. Andreev, Importance of the Breit interaction for calculation of the differential cross section for dielectronic recombination with one-electron uranium, Phys. Rev. A **91**, 012511 (2015).

[11] S. Zakowicz, W. Scheid, and N. Grün, Dielectronic recombination into hydrogen-like heavy ions with emission of two photons, J. Phys. B **37**, 131 (2004).

[12] N. Nakamura, A. P. Kavanagh, H. Watanabe, H. A. Sakaue, Y. Li, D. Kato, F. J. Currell, and S. Ohtani, Evidence for strong Breit interaction in dielectronic recombination of highly charged heavy ions, Phys. Rev. Lett. **100**, 073203 (2008).

[13] S. Mahmood, S. Ali, I. Orban, S. Tashenov, E. Lindroth, and R. Schuch, Recombination and electron impact excitation rate coefficients for S XV and S XVI, Astrophys. J. **754**, 86 (2012).

[14] E. Lindroth, I. Orban, S. Trotsenko, and R. Schuch, Electron-impact recombination and excitation rates for charge-state-selected highly charged Si ions, Phys. Rev. A **101**, 062706 (2020).

[15] Z. Hu, G. Xiong, Z. He, Z. Yang, N. Numadate, C. Huang, J. Yang, K. Yao, B. Wei, Y. Zou, C. Wu, Y. Ma, Y. Wu, X. Gao, and N. Nakamura, Giant retardation effect in electron-electron interaction, Phys. Rev. A **105**, L030801 (2022).

[16] F. Aharonian *et al.* (Hitomi Collaboration), Atomic data and spectral modeling constraints from high-resolution X-ray observations of the Perseus cluster with Hitomi, Publ. Astron. Soc. Jpn. **70**, 12 (2018).

[17] O. Y. Andreev, L. N. Labzowsky, G. Plunien, and D. A. Solovyev, QED theory of the spectral line profile and its applications to atoms and ions, Phys. Rep. **455**, 135 (2008).

[18] D. A. Varshalovich, A. N. Moskalev, and V. K. Khersonskii, *Quantum Theory of Angular Momentum* (World Scientific, Singapore, 1988).

[19] O. Y. Andreev, L. N. Labzowsky, and A. V. Prigorovsky, Line-profile approach to the description of the electron-recombination process for the highly charged ions, Phys. Rev. A **80**, 042514 (2009).

[20] V. M. Shabaev, I. I. Tupitsyn, and V. A. Yerokhin, Model operator approach to the Lamb shift calculations in relativistic many-electron atoms, Phys. Rev. A **88**, 012513 (2013).

[21] W. R. Johnson, S. A. Blundell, and J. Sapirstein, Finite basis sets for the Dirac equation constructed from B splines, Phys. Rev. A **37**, 307 (1988).

[22] V. M. Shabaev, I. I. Tupitsyn, V. A. Yerokhin, G. Plunien, and G. Soff, Dual kinetic balance approach to basis-set expansions for the Dirac equation, Phys. Rev. Lett. **93**, 130405 (2004).